ORIGINAL ARTICLE

Trabecular bone structure analysis of the spine using clinical MDCT: can it predict vertebral bone strength?

**Thomas Baum · Martin Gräbeldinger · Christoph Räth · Eduardo Grande Garcia ·
Rainer Burgkart · Janina M. Patsch · Ernst J. Rummeny · Thomas M. Link ·
Jan S. Bauer**

Abstract Recent technical improvements have made it possible to determine trabecular bone structure parameters of the spine using clinical multi-detector computed tomography (MDCT). Therefore, the purpose of this study was to analyze trabecular bone structure parameters obtained from clinical MDCT in relation to high resolution peripheral quantitative computed tomography (HR-pQCT) as a standard of reference and to investigate whether clinical MDCT can predict vertebral bone strength. Fourteen functional spinal segment units between T7 and L3 were harvested from 14 formalin-fixed human cadavers (11 women and 3 men; age 84 ± 10 years). All functional spinal segment units were examined using HR-pQCT (isotropic voxel size of 41 μm^3) and a clinical whole-body MDCT (interpolated voxel size of $146 \times 146 \times 300$ μm^3). Trabecular bone structure analyses (histomorphometric and texture measures) were performed in the HR-pQCT as well as MDCT images. Vertebral failure load (FL) of the functional spinal segment units was determined in an uniaxial biomechanical test. The HR-pQCT and MDCT derived trabecular bone structure parameters showed correlations ranging from $r = 0.60$ to $r = 0.90$ ($p < 0.05$). Correlations between trabecular bone structure parameters and FL amounted up to $r = 0.86$ ($p < 0.05$) using the HR-pQCT images, and up to $r = 0.79$ ($p < 0.05$) using the MDCT images. Correlation coefficients of FL versus trabecular bone structure parameters obtained with HR-pQCT and MDCT were not significantly different ($p > 0.05$). In this cadaver model, the spatial resolution of clinically available whole-body MDCT scanners was suitable for trabecular bone structure analysis of the spine and to predict vertebral bone strength.

Keywords Osteoporosis · Vertebral bone strength · HR-pQCT · MDCT · Trabecular bone structure

T. Baum (✉) · M. Gräbeldinger · E. Grande Garcia ·
E. J. Rummeny · J. S. Bauer
Institut für Radiologie, Klinikum rechts der Isar, Technische
Universität München, Ismaninger Str. 22, 81675 Munich,
Germany
e-mail: thbaum@gmx.de

C. Räth
Max-Planck-Institut für extraterrestrische Physik,
Giessenbachstr. 1, 85748 Garching, Germany

E. Grande Garcia · R. Burgkart
Klinik für Orthopädie und Sportorthopädie, Abteilung für
Biomechanik, Klinikum rechts der Isar, Technische Universität
München, Ismaninger Str. 22, 81675 Munich, Germany

J. M. Patsch
Universitätsklinik für Radiodiagnostik, Medizinische Universität
Wien, Währinger Gürtel 18-20, 1090 Vienna, Austria

T. M. Link
Musculoskeletal and Quantitative Imaging Research Group,
Department of Radiology and Biomedical Imaging, University
of California San Francisco, 185 Berry Street, Suite 350,
San Francisco, CA 94107, USA

Introduction

Osteoporosis is defined as a skeletal disorder characterized by compromised bone strength predisposing an individual to an increased risk of fracture [1]. Due to the aging population, osteoporosis is classified as a public health problem [2, 3]. Osteoporotic fractures are associated with a high morbidity and mortality, and generate immense financial cost [4–7]. Therefore, different methods have been established to identify patients at high risk of osteoporotic fractures and to initiate appropriate therapy before osteoporosis associated fractures occur. Imaging based methods include dual-energy X-ray

absorptiometry (DXA) and quantitative computed tomography (QCT) of the spine and hip measuring bone mineral density (BMD) [8, 9]. The World Health Organisation (WHO) definition of osteoporosis is based on the DXA derived T score [10]. However, T scores and BMD values of patients with and without osteoporotic fractures overlap [11, 12]. Therefore, the Fracture Risk Assessment Tool (FRAX) has been introduced, which uses easily obtainable clinical risk factors to estimate 10-year fracture probability in order to provide a clinical guidance for treatment decisions [13, 14]. Furthermore, advanced imaging techniques have been developed focusing on the assessment of bone quality, which is in addition to BMD an important parameter for predicting bone strength [15–17]. Bone quality can be partly assessed by analyzing the trabecular bone architecture. It was reported previously that trabecular bone structure parameters could add significant information beyond BMD for predicting bone strength and evaluating therapy response in osteoporosis [18–24]. Since high resolution image acquisition is required for trabecular bone structure analysis, assessment of the trabecular bone architecture at the spine was limited in the past due to the spatial resolution of clinically available whole body multi-detector computed tomography (MDCT) scanners. However, the spine is one of the most important osteoporotic fracture sites. Therefore, trabecular bone structure analysis at the spine may be beneficial for fracture risk prediction and therapy monitoring.

Recent technical improvements have made it possible to determine trabecular bone structure parameters of the spine using clinical MDCT. Issever et al. [25] reported high correlations between micro-computed tomography (μCT) and MDCT derived trabecular bone structure parameters at the lumbar spine ex vivo. While this study did not perform a biomechanical testing, Bauer et al. [26] demonstrated that μCT and MDCT derived trabecular bone structure parameters of bone probes harvested from the thoracic spine showed similar correlations with biomechanically determined bone strength. However, it remains to be investigated whether these findings are valid for whole vertebra and functional spinal segment units.

Therefore, the purpose of this study was to analyze trabecular bone structure parameters obtained from clinical MDCT in relation to HR-pQCT (high resolution peripheral quantitative computed tomography) as a standard of reference in functional spinal segment units and to investigate whether clinical MDCT can predict vertebral bone strength.

Materials and methods

Specimens

Our study was designed to biomechanically test functional spinal segment units with intact ligaments, intervertebral
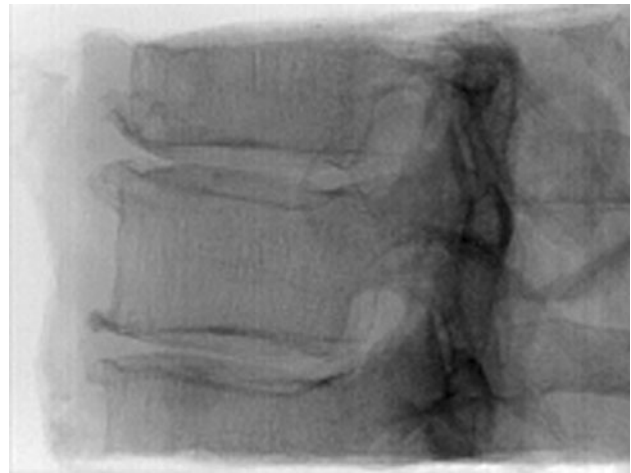

Fig. 1 Representative X-ray image of a functional spinal segment unit with intact ligaments, intervertebral discs, and posterior elements of the thoracic spine

discs, and posterior elements. Therefore, 14 spinal 3-segment units between T7 and L3 were harvested from 14 formalin-fixed human cadavers (11 women and 3 men; mean age ± SD of 84 ± 10 years). The spinal 3-segment units consisted of one T7–T9 unit, one T8–T10 unit, four T9–T11 units, two T10–T12 units, three T11–L1 units, one T12–L2 unit, and two L1–L3 units. The donors had dedicated their body for educational and research purposes to the local Institute of Anatomy prior to death, in compliance with local institutional and legislative requirements. The study protocol was reviewed and approved by the local Institutional Review Boards. Donors with a history of pathological bone changes other than osteoporosis (i.e., bone metastases, hematological, or metabolic bone disorders) were excluded at the outset. Surrounding muscle and fat tissue was completely removed from the spinal 3-segment units. Then half of the upper and lower vertebra of the spinal 3-segment units was removed with a band saw to create functional spinal segment units with intact ligaments, intervertebral discs, and posterior elements. In case of thoracic segment units, the costovertebral joints were kept intact by dissecting the costae distally of the costovertebral joints. A representative X-ray image of a functional spinal segment unit is shown in Fig. 1. For the purpose of conservation, all functional spinal segment units were stored in formalin solution during the study and degassed at least 24 h before imaging to prevent air artifacts. The functional spinal segment units were sealed in vacuum plastic bags during imaging.

Imaging

The MDCT images of the functional spinal segment units were acquired by using a whole-body 256-row CT scanner
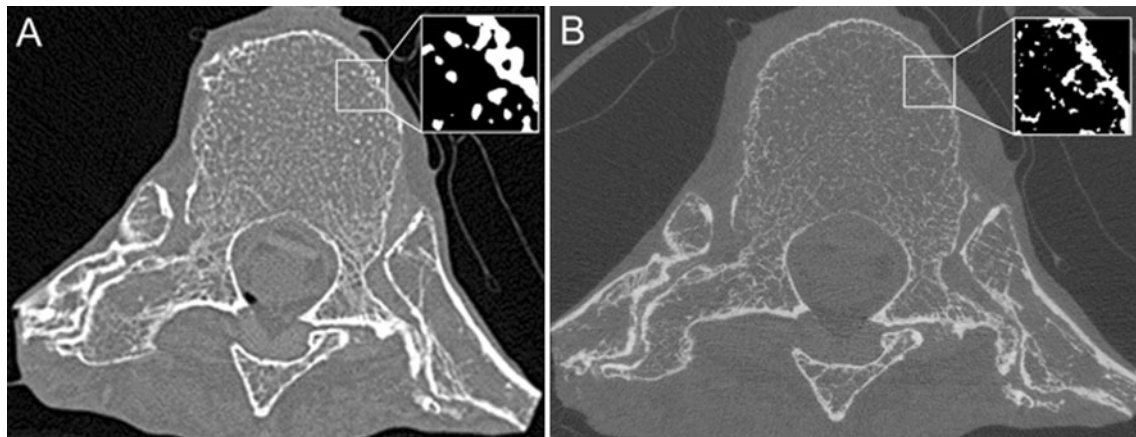
Fig. 2 Corresponding MDCT (**a**) and HR-pQCT (**b**) images of a representative functional spinal segment unit. The *insets* show an enlarged region after binarization to better appreciate the different spatial resolution

(iCT, Philips Medical Care, Best, The Netherlands). Scan parameters were a tube voltage of 120 kVp, a tube load of 585 mAs, an image matrix of 1024 × 1024 pixels, and a field of view of 150 mm. Transverse sections were reconstructed with a high-resolution bone kernel (YE). The interpolated voxel size was of $146 \times 146 \times 300$ μm^3, while the real spatial resolution, as determined at ρ50 of the modulation-transfer-function, was $250 \times 250 \times 600$ μm^3. A dedicated calibration phantom (Mindways Osteoporosis Phantom, San Francisco, CA, USA) was placed in the scanner mat beneath the functional spinal segment units.

The HR-pQCT scans of the functional spinal segment units were performed with a XtremeCT system (SCANCO Medical AG, Brüttiselen, Switzerland). A standard protocol with a tube voltage of 60 kVp and a tube load of 180 μmAs was used and transverse sections with an isotropic voxel size of 41 μm^3 were reconstructed. The intensity values of HR-pQCT images were calibrated with a reference phantom to derive calcium hydroxyapatite values in (mg/cm^3).

Corresponding MDCT and HR-pQCT images of a representative functional spinal segment unit are shown in Fig. 2.

Image analysis

All acquired images were transferred to a remote LINUX workstation. An in-house developed algorithm based on IDL (Interactive Data Language, Research Systems, Bolder, CO, USA) was used for image analysis. The MDCT and HR-pQCT images of each functional spinal segment unit were opened in separate image panels at the same time. The operator identified visually the slice of the middle vertebra equidistant to its endplates in the MDCT and HR-pQCT images. Subsequently, the 20 and 150 most

central slices of the middle vertebra were selected in the MDCT and HR-pQCT images, respectively. Twenty oval regions of interest (ROIs) were manually placed at once in the ventral half of the middle vertebra of the functional spinal segment unit in the selected slices of the MDCT images by using a batch process. The placement of the ROIs was similarly performed in the selected 150 slices of the HR-pQCT images. The operator matched the position of ROIs in MDCT and HR-pQCT images visually in the simultaneously opened image panels. Dependent on the vertebral level of the functional spinal segment units, the size of oval ROI was adjusted accordingly with a length varying between 24 and 35 mm and a width varying between 15 and 26 mm. The length and width of the oval ROIs were identical in corresponding MDCT and HR-pQCT images of each functional spinal segment. Standard QCT-derived BMD measurements are usually performed in a 8–10 mm slice in L1–L3 covering the central third of the vertebral height [8]. Since the functional spinal segment units were in the majority harvested from the thoracic spine, we decided to reduce the height of the ROIs to about 6 mm (i.e., 20 and 150 slices of the MDCT and HR-pQCT images, respectively) to account for smaller heights of the thoracic vertebrae. In addition, ROIs were drawn in two phases of the Mindways calibration phantom in the MDCT images (Fig. 3).

Binarization of the MDCT and HR-pQCT images was required to compute morphometric parameters of the trabecular bone structure. For this purpose, we applied an optimized global threshold to all images. To determine this threshold, we evaluated the MDCT and HR-pQCT images of five randomly selected functional spinal segment units visually. The best threshold was found to be 200 mg/cm^3 calcium hydroxyapatite similar to previous studies [18, 19, 26]. By using this threshold, functional spinal segment units with dense trabecular bone structure did not only
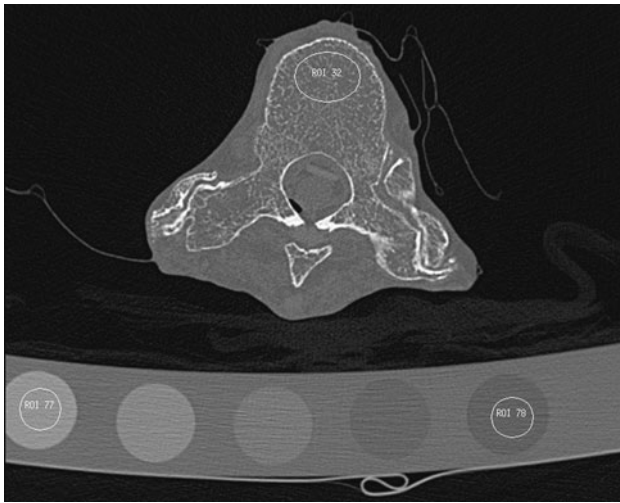
Fig. 3 Representative MDCT image of the functional spinal segment unit: an oval region of interest (ROI) was placed in the ventral half of the middle vertebra of the functional spinal segment unit. In addition, ROIs were drawn in two phases of the Mindways calibration phantom in the MDCT images. The ROIs were positioned in the 20 most central slices of the middle vertebra in the MDCT images and correspondingly in the 150 most central slices of the middle vertebra in the HR-pQCT images

consist of "bone" voxels and osteoporotic functional spinal segment units still showed trabecular structure and not only "marrow" voxels. After binarization, four morphometric parameters were calculated in the ROIs in analogy to standard histomorphometry using the mean intercept length method [27]: bone volume divided by total volume (BV/TV), trabecular number [TbN (mm^{-1})], trabecular separation [TbSp (mm)], and trabecular thickness [TbTh (mm)].

In addition, fractal dimension (FD) as texture measurement of the trabecular bone structure was determined in the MDCT and HR-pQCT images using a box counting algorithm as previously described [28, 29].

Lastly, mean BMD of each ROI was calculated in the MDCT images by converting the pixel attenuations in (HU; Hounsfield Units) into BMD values in (mg/cm^3) by using the Mindways calibration phantom as outlined previously [30].

All steps of the image analysis were performed by one operator.

Biomechanical testing

The half-dissected upper and lower vertebrae of the functional spinal segment units were embedded in resin (Rencast Isocyanat and Polyol, Huntsman Group, Bad Säckingen, Germany) up to 2 mm above, respectively, below their vertebral endplates. The fixation was performed with parallel alignment of the upper and lower endplate of middle vertebra with the outer surface of the resin chock to guarantee strict axial loading conditions of the middle vertebra during the uniaxial biomechanical test. After embedding, the functional spinal segment units were fixed in a mechanical testing system (Wolpert Werkstoffprüfmaschinen AG, Schaffhausen, Switzerland). Similar to previous studies [31, 32], ten pre-conditioning cycles with uniaxial tension–compression up to a load between 10 and 400 N with a rate of 5 mm/min was applied. Then a monotonic, uniaxial compression was performed at the same rate. The load–displacement curve was recorded and vertebral failure load (FL) was defined as the first peak of the load–displacement curve with a subsequent drop of >10 % as outlined previously [33].

Statistical analysis

The statistical analyses were performed with SPSS (SPSS, Chicago, IL, USA). All tests were done using a two-sided 0.05 level of significance.

Mean and SD of all parameters were calculated for all functional spinal segment units. The Kolmogorov–Smirnov test showed for all parameters no significant difference from a normal distribution ($p > 0.05$). Therefore, differences between MDCT and HR-pQCT derived trabecular bone structure parameters were assessed with paired t tests. Correlations between two parameters were evaluated with the Pearson product-moment correlation coefficient (r). Significant differences between correlation coefficients were assessed using the Fisher Z transformation. Furthermore, correlations between MDCT as well as HR-pQCT derived parameters versus FL were adjusted for BMD using partial correlation analysis.

Reproducibility

Five functional spinal segment units were randomly selected to assess the reproducibility error of BMD and trabecular bone structure parameters. The ROIs were placed three times by one operator in the MDCT and HR-pQCT images. Corresponding BMD as well as trabecular bone structure parameters were calculated each time in the MDCT and HR-pQCT images, respectively. Reproducibility errors were computed as the root mean square error coefficient of variation according to Gluer et al. [34] and amounted to 1.2 % for BMD, 1.9 and 2.4 % for MDCT and HR-pQCT derived BV/TV, 1.2 and 1.0 % for MDCT and HR-pQCT derived TbN, 0.9 and 1.1 % for MDCT and HR-pQCT derived TbSp, 2.0 and 2.5 % for MDCT and HR-pQCT derived TbTh, and 0.5 and 0.4 % for MDCT and HR-pQCT derived FD, respectively.

Results

Mean ± SD of FL and BMD of all functional spinal segment units amounted to 3243 ± 1071 N and 57.4 ± 20.4 mg/cm³, respectively. Corresponding values of MDCT as well as HR-pQCT derived trabecular bone structure parameters of all functional spinal segment units are listed in Table 1. The BV/TV, TbSp, and TbTh were significantly greater, while TbN was significantly lower in the MDCT images compared to the corresponding HR-pQCT images ($p < 0.001$; Table 1). Values of FD derived from MDCT and HR-pQCT were not significantly different ($p = 0.703$; Table 1). Except for TbTh, MDCT and HR-pQCT derived trabecular bone structure parameters showed significant correlations with Pearson product-moment correlation coefficients ranging from $r = 0.60$ to $r = 0.90$ (Table 2).

Correlations of the trabecular bone structure parameters with FL amounted up to $r = 0.86$ ($p < 0.05$) using the HR-pQCT images, and up to $r = 0.79$ ($p < 0.05$) using the MDCT images (Table 2). The greatest correlations were observed for MDCT derived BV/TV and HR-pQCT

derived TbN, while neither MDCT nor HR-pQCT derived TbTh showed significant correlations with FL ($p > 0.05$; Table 2). Correlation coefficients of FL versus trabecular bone structure parameters obtained with HR-pQCT and MDCT were not significantly different as assessed by the Fisher Z transformation ($p > 0.05$).

The BMD significantly correlated with FL ($r = 0.75$; $p = 0.008$). The correlation coefficients of FL versus the best trabecular bone structure parameters derived from both, HR-pQCT and MDCT, were not significantly different from the correlation coefficient of FL versus BMD ($p > 0.05$). The HR-pQCT as well as MDCT derived trabecular bone structure parameters showed high correlations with BMD (up to $r = 0.82$; $p < 0.001$ and up to $r = 0.92$; $p < 0.001$, respectively).

Correlations between MDCT as well as HR-pQCT derived trabecular bone structure parameters versus FL adjusted for BMD are displayed in Table 2. After adjustment for BMD, only HR-pQCT derived TbN and TbTh showed statistically significant correlations with FL ($r = 0.70$; $p = 0.025$ and $r = 0.66$; $p = 0.038$, respectively).

Table 1 Mean ± SD of MDCT as well as HR-pQCT derived trabecular bone structure parameters as well as MDCT derived BMD of all functional spinal segment units ($n = 14$)

	MDCT	HR-pQCT	p value
BV/TV	0.130 ± 0.044	0.072 ± 0.031	<0.001
TbN (mm)	0.557 ± 0.163	1.103 ± 0.493	<0.001
TbSp (mm)	1.725 ± 0.627	1.106 ± 0.707	<0.001
TbTh (mm)	0.231 ± 0.021	0.066 ± 0.014	<0.001
FD	1.380 ± 0.134	1.384 ± 0.110	0.703
BMD (mg/cm³)	57.4 ± 20.4	–	–

Differences between corresponding MDCT and HR-pQCT derived parameters were assessed with paired t tests. Statistical significance is indicated by p values <0.05

Discussion

In this study, MDCT and HR-pQCT derived trabecular bone structure parameters assessed in functional spinal segment units showed high correlations despite the different spatial resolutions of the MDCT and HR-pQCT protocols. Furthermore, HR-pQCT as well as MDCT derived trabecular bone structure parameters adequately predicted biomechanically determined vertebral bone strength.

High-resolution trabecular bone imaging yields additional information beyond BMD to predict bone strength [15–17]. While HR-pQCT is limited to peripheral skeletal sites such as the distal radius and tibia in vivo, magnetic resonance imaging (MRI) showed promising results at the

Table 2 Pearson product-moment correlation coefficient r (p value) of MDCT versus HR-pQCT derived trabecular bone structure parameters, and MDCT as well as HR-pQCT derived parameters versus failure load (FL), respectively

	MDCT vs. HR-pQCT	MDCT vs. FL	MDCT vs. FL adjusted for BMD	HR-pQCT vs. FL	HR-pQCT vs. FL adjusted for BMD
BV/TV	0.90 (**$p < 0.001$**)	0.79 (**$p = 0.004$**)	0.40 ($p = 0.259$)	0.69 (**$p = 0.020$**)	0.18 ($p = 0.614$)
TbN (mm)	0.78 (**$p = 0.001$**)	0.73 (**$p = 0.011$**)	0.12 ($p = 0.735$)	0.86 (**$p = 0.001$**)	0.70 (**$p = 0.025$**)
TbSp (mm)	0.90 (**$p < 0.001$**)	−0.77 (**$p = 0.006$**)	−0.29 ($p = 0.416$)	−0.84 (**$p = 0.001$**)	−0.58 ($p = 0.079$)
TbTh (mm)	0.06 ($p = 0.836$)	0.60 ($p = 0.053$)	0.52 ($p = 0.125$)	0.32 ($p = 0.345$)	0.66 (**$p = 0.038$**)
FD	0.60 (**$p = 0.038$**)	0.69 (**$p = 0.018$**)	0.12 ($p = 0.738$)	0.85 (**$p = 0.003$**)	0.68 ($p = 0.061$)
BMD (mg/cm³)	–	0.75 (**$p = 0.008$**)	–	–	–

Correlations between MDCT as well as HR-pQCT derived parameters versus FL were also adjusted for BMD using partial correlation analysis. Statistical significance is indicated by p values <0.05 and corresponding values are displayed in bold

proximal femur [35, 36]. However, high-resolution trabecular bone imaging at the spine as a clinically important osteoporotic fracture site is limited to MDCT in vivo. Since trabeculae have a diameter between 50 and 200 μm, the spatial resolution of the whole-body MDCT scanners is critical for trabecular bone structure analysis. Due to recent technical developments, trabeculae can be depicted by clinically available MDCT systems. Results of previous studies underlined the importance to compute trabecular bone structure parameters and finite element models (FEM) at the spine for predicting vertebral fracture risk and monitoring therapy response [37–40].

However, little is known about the required spatial resolution for adequate trabecular bone structure analysis and corresponding prediction of vertebral bone strength using MDCT. Issever et al. [41] reported that 64- and 320-slice MDCT systems both performed equally well in depicting trabecular bone architecture at the distal radius. Furthermore, they observed high correlations between μCT and MDCT derived trabecular bone structure parameters at the lumbar spine ex vivo [25]. However, they compared the calculated trabecular bone structure parameters with μFEM-derived bone properties and did not perform a biomechanical testing.

Bauer et al. [26] demonstrated that μCT and MDCT derived trabecular bone structure parameters showed similar correlations with biomechanically determined bone strength. They investigated bone probes harvested from the thoracic spine, but not whole vertebrae or functional spinal segment units, which is a limitation of their study. In our study, we harvested functional spinal segment units to design an experimental setup simulating the biomechanical in vivo conditions of the spine as close as possible.

The absolute values of the MDCT and HR-pQCT derived histomorphometric parameters were significantly different. Thus, the absolute values are affected by the different spatial resolution of MDCT and HR-pQCT. In contrast to the histomorphometric parameters, the values of FD as assessed by MDCT and HR-pQCT were not statistically significantly different. Due to its calculation using a box counting algorithm, FD seems to be more robust with respect to spatial resolution than standard histomorphometry. The MDCT derived trabecular bone structure parameters correlated well with HR-pQCT derived parameters, BMD, and biomechanically determined FL. The sole exception was ThTh; not only MDCT but also HR-pQCT derived TbTh showed no significant correlation with FL. The TbTh was apparently less suitable for predicting bone strength in our sample size consisting of 14 functional spinal segment units. However, TbTh showed promising results in previous studies at the spine, hip, and distal radius [18, 20, 25]. Furthermore, HR-pQCT derived

TbTh correlated well with FL after adjusting for BMD ($r = 0.66$; $p = 0.038$). Thus, out of all histomorphometric parameters, TbTh may be most affected by BMD as well as by the spatial resolution, since the correlation of MDCT and HR-pQCT derived TbTh was also not statistically significant.

It is important to note that only HR-pQCT derived TbN and TbTh showed statistically significant correlations with FL after adjustment for BMD ($r = 0.70$; $p = 0.025$ and $r = 0.66$; $p = 0.038$, respectively). These findings underline the considerable contribution of BMD to bone strength. In this study population, HR-pQCT derived trabecular bone structure analysis predicted independent of BMD vertebral bone strength, in contrast to MDCT derived trabecular bone structure parameters. Nevertheless, our findings suggest that the spatial resolution of clinically available whole-body MDCT scanners is suitable for trabecular bone structure analysis of the spine and to predict vertebral bone strength. However, the prediction of bone strength by MDCT derived trabecular bone structure parameters was dependent on BMD as assessed by the partial correlation analysis adjusting for BMD.

The comparison of MDCT derived trabecular bone structure parameters and those obtained with HR-pQCT or μCT as standard of reference has always take into account potential error sources introduced by image analysis steps. Most critical is the optimization process of the applied global threshold for the binarization of the images. Issever et al. [25] assessed trabecular bone structure parameters in the spine using clinical MDCT and compared them with those obtained by μCT. They used a common adaptive iterative method on a specific specimen-based histogram analysis to determine the threshold for the binarization of the μCT images. Six different global thresholds were applied on the MDCT images. They identified the optimal MDCT threshold by correlating μCT and MDCT derived trabecular bone structure parameters. The MDCT threshold that yielded the highest correlation coefficients of μCT and MDCT derived trabecular bone structure parameters was finally considered as optimal threshold. We used a different approach in this study. Although the spatial resolution was different for MDCT and HR-pQCT, we selected the same optimized threshold for both imaging modalities. Thus, our threshold was not based on a statistical analysis, but on the visual image impression resulting from the applied threshold. This may be advantageous, since our approach was not result-driven with respect to achieve best possible correlation coefficients, but visually evaluated the effect of the applied threshold on the images. Furthermore, the absolute values of our HR-pQCT derived trabecular bone structure parameters were similar to those reported by Issever et al. [25] and Bauer et al. [26], who derived these

parameters by using μCT imaging in comparable study populations. This indicates that our selected optimized global threshold for both, MDCT and HR-pQCT, can be considered as well chosen.

We only assessed trabecular bone structure parameters in this study. However, it is well known that the cortical compartment contributes substantially to the mechanical properties of the bone [42]. Cortical bone structure parameters such as endplate thickness were good predictors of vertebral strength [43]. Measurements of cortical thickness or surface area can be obtained at the spine in vivo by using MDCT [8, 17]. However, advanced cortical bone structure parameters including cortical porosity as assessed at the distal radius and tibia in vivo by using HR-pQCT are technically not feasible at the spine by using MDCT due to the limited spatial resolution [36].

Our MDCT protocol has to be optimized for in vivo application. Graeff et al. [39] performed high-resolution MDCT imaging of T12 or L1 to monitor teriparatide associated changes in vertebral bone structure. They used a tube voltage of 120 kV and a tube load of 360 mAs. The estimated dose equivalent amounted to 3 mSv. If we optimize our protocol for in vivo application, it would be probably close to that reported by Graeff et al. This dose equivalent may be regarded as a dose in the upper range of medically indicated radiation exposure. Therefore, trabecular bone structure analysis using high-resolution MDCT cannot be applied for osteoporosis diagnostics and therapy monitoring in clinical routine at the moment. Only patients with borderline pathological BMD values or subjects included in specific drug trials may benefit from the assessment of trabecular bone structure at the spine using MDCT. Consequently, radiation dose reduction by newly developed CT reconstruction algorithms, e.g., iterative reconstruction, are needed in the future [44]. Furthermore, technical developments may improve the achievable spatial resolution. Flat-panel CT devices have been developed recently and offer higher spatial resolutions than MDCT of up to 150 μm isotropic due to the high number of pixels [45].

Our study had some limitations. Firstly, MDCT scanning was not performed with a torso phantom to simulate a soft tissue environment as outlined previously for MDCT scans at the proximal femur [46]. Soft tissue scatter may compromise the image quality. This may impact the ability to extrapolate our results to a clinical in vivo setting and remains to be investigated in future studies. Secondly, the functional spinal segment units were harvested from formalin-fixed cadavers, which may have affected the biomechanical properties, and the HR-pQCT as well as MDCT measurements. However, a previous study reported that dual energy DXA derived BMD measurements were not significantly affected by fixation [47]. Thirdly, FD was

the only advanced trabecular bone structure parameter computed in this study in addition to standard histomorphometric parameters. However, the focus of this study was on the experimental setup using functional spinal segment units and not on the calculation of various trabecular bone structure parameters. Lastly, important risk factors as enquired in the FRAX were not considered in this in vitro study, but are important to determine the fracture risk in vivo [13].

In conclusion, the spatial resolution of clinically available whole-body MDCT scanners was suitable for trabecular bone structure analysis of the spine and to predict vertebral bone strength in this cadaver study. Simulations with torso phantoms and radiation dose reduction by newly developed CT reconstruction algorithms, e.g., iterative reconstruction, are needed in the future to reliably assess trabecular bone structure parameters at the spine in vivo by using clinical MDCT.

Conflict of interest The authors state no conflict of interest.

References

1. NIH Consensus Development Panel on Osteoporosis Prevention, Diagnosis, and Therapy (2001) Highlights of the conference. South Med J 94:569–573
2. Schuiling KD, Robinia K, Nye R (2011) Osteoporosis update. J Midwifery Womens Health 56:615–627
3. Cole ZA, Dennison EM, Cooper C (2008) Osteoporosis epidemiology update. Curr Rheumatol Rep 10:92–96
4. Ioannidis G, Papaioannou A, Hopman WM, Akhtar-Danesh N, Anastassiades T, Pickard L, Kennedy CC, Prior JC, Olszynski WP, Davison KS, Goltzman D, Thabane L, Gafni A, Papadimitropoulos EA, Brown JP, Josse RG, Hanley DA, Adachi JD (2009) Relation between fractures and mortality: results from the Canadian Multicentre Osteoporosis Study. CMAJ 181:265–271
5. Papaioannou A, Kennedy CC, Ioannidis G, Sawka A, Hopman WM, Pickard L, Brown JP, Josse RG, Kaiser S, Anastassiades T, Goltzman D, Papadimitropoulos M, Tenenhouse A, Prior JC, Olszynski WP, Adachi JD (2009) The impact of incident fractures on health-related quality of life: 5 years of data from the Canadian Multicentre Osteoporosis Study. Osteoporos Int 20:703–714
6. Adachi JD, Loannidis G, Berger C, Joseph L, Papaioannou A, Pickard L, Papadimitropoulos EA, Hopman W, Poliquin S, Prior JC, Hanley DA, Olszynski WP, Anastassiades T, Brown JP, Murray T, Jackson SA, Tenenhouse A (2001) The influence of osteoporotic fractures on health-related quality of life in community-dwelling men and women across Canada. Osteoporos Int 12:903–908
7. Leboime A, Confavreux CB, Mehsen N, Paccou J, David C, Roux C (2010) Osteoporosis and mortality. Jt Bone Spine 77:107–112
8. Adams JE (2009) Quantitative computed tomography. Eur J Radiol 71:415–424
9. Blake GM, Fogelman I (2009) The clinical role of dual energy X-ray absorptiometry. Eur J Radiol 71:406–414

10. WHO Study Group (1994) Assessment of fracture risk and its application to screening for postmenopausal osteoporosis. Report of a WHO Study Group. World Health Organ Tech Rep Ser 843:1–129

11. Schuit SC, van der Klift M, Weel AE, de Laet CE, Burger H, Seeman E, Hofman A, Uitterlinden AG, van Leeuwen JP, Pols HA (2004) Fracture incidence and association with bone mineral density in elderly men and women: the Rotterdam Study. Bone 34:195–202

12. Siris ES, Chen YT, Abbott TA, Barrett-Connor E, Miller PD, Wehren LE, Berger ML (2004) Bone mineral density thresholds for pharmacological intervention to prevent fractures. Arch Intern Med 164:1108–1112

13. McCloskey E, Johansson H, Oden A, Kanis JA (2012) Fracture risk assessment. Clin Biochem 45:887–893

14. Kanis JA, Oden A, Johansson H, Borgstrom F, Strom O, McCloskey E (2009) FRAX and its applications to clinical practice. Bone 44:734–743

15. Bauer JS, Link TM (2009) Advances in osteoporosis imaging. Eur J Radiol 71:440–449

16. Ito M (2011) Recent progress in bone imaging for osteoporosis research. J Bone Miner Metab 29:131–140

17. Link TM (2012) Osteoporosis imaging: state of the art and advanced imaging. Radiology 263:3–17

18. Bauer JS, Kohlmann S, Eckstein F, Mueller D, Lochmuller EM, Link TM (2006) Structural analysis of trabecular bone of the proximal femur using multislice computed tomography: a comparison with dual X-ray absorptiometry for predicting biomechanical strength in vitro. Calcif Tissue Int 78:78–89

19. Baum T, Carballido-Gamio J, Huber MB, Muller D, Monetti R, Rath C, Eckstein F, Lochmuller EM, Majumdar S, Rummeny EJ, Link TM, Bauer JS (2010) Automated 3D trabecular bone structure analysis of the proximal femur-prediction of biomechanical strength by CT and DXA. Osteoporos Int 21:1553–1564

20. Baum T, Kutscher M, Muller D, Rath C, Eckstein F, Lochmuller EM, Rummeny EJ, Link TM, Bauer JS (2013) Cortical and trabecular bone structure analysis at the distal radius-prediction of biomechanical strength by DXA and MRI. J Bone Miner Metab 31:212–221

21. Hudelmaier M, Kollstedt A, Lochmuller EM, Kuhn V, Eckstein F, Link TM (2005) Gender differences in trabecular bone architecture of the distal radius assessed with magnetic resonance imaging and implications for mechanical competence. Osteoporos Int 16:1124–1133

22. Link TM, Majumdar S, Lin JC, Augat P, Gould RG, Newitt D, Ouyang X, Lang TF, Mathur A, Genant HK (1998) Assessment of trabecular structure using high resolution CT images and texture analysis. J Comput Assist Tomogr 22:15–24

23. Link TM, Majumdar S, Lin JC, Newitt D, Augat P, Ouyang X, Mathur A, Genant HK (1998) A comparative study of trabecular bone properties in the spine and femur using high resolution MRI and CT. J Bone Miner Res 13:122–132

24. Greenspan SL, Perera S, Recker R, Wagner JM, Greeley P, Gomberg BR, Seaman P, Kleerekoper M (2010) Changes in trabecular microarchitecture in postmenopausal women on bisphosphonate therapy. Bone 46:1006–1010

25. Issever AS, Link TM, Kentenich M, Rogalla P, Schwieger K, Huber MB, Burghardt AJ, Majumdar S, Diederichs G (2009) Trabecular bone structure analysis in the osteoporotic spine using a clinical in vivo setup for 64-slice MDCT imaging: comparison to microCT imaging and microFE modeling. J Bone Miner Res 24:1628–1637

26. Bauer JS, Issever AS, Fischbeck M, Burghardt A, Eckstein F, Rummeny EJ, Majumdar S, Link TM (2004) Multislice-CT for structure analysis of trabecular bone—a comparison with micro-CT and biomechanical strength. Rofo 176:709–718

27. Parfitt AM, Drezner MK, Glorieux FH, Kanis JA, Malluche H, Meunier PJ, Ott SM, Recker RR (1987) Bone histomorphometry: standardization of nomenclature, symbols, and units. Report of the ASBMR Histomorphometry Nomenclature Committee. J Bone Miner Res 2:595–610

28. Majumdar S, Genant HK, Grampp S, Newitt DC, Truong VH, Lin JC, Mathur A (1997) Correlation of trabecular bone structure with age, bone mineral density, and osteoporotic status: in vivo studies in the distal radius using high resolution magnetic resonance imaging. J Bone Miner Res 12:111–118

29. Baum T, Dutsch Y, Muller D, Monetti R, Sidorenko I, Rath C, Rummeny EJ, Link TM, Bauer JS (2012) Reproducibility of trabecular bone structure measurements of the distal radius at 1.5 and 3.0 T magnetic resonance imaging. J Comput Assist Tomogr 36:623–626

30. Huber MB, Carballido-Gamio J, Bauer JS, Baum T, Eckstein F, Lochmuller EM, Majumdar S, Link TM (2008) Proximal femur specimens: automated 3D trabecular bone mineral density analysis at multidetector CT-correlation with biomechanical strength measurement. Radiology 247:472–481

31. Chevalier Y, Charlebois M, Pahra D, Varga P, Heini P, Schneider E, Zysset P (2008) A patient-specific finite element methodology to predict damage accumulation in vertebral bodies under axial compression, sagittal flexion and combined loads. Comput Methods Biomech Biomed Eng 11:477–487

32. Dall'Ara E, Pahr D, Varga P, Kainberger F, Zysset P (2012) QCT-based finite element models predict human vertebral strength in vitro significantly better than simulated DEXA. Osteoporos Int 23:563–572

33. Burklein D, Lochmuller E, Kuhn V, Grimm J, Barkmann R, Muller R, Eckstein F (2001) Correlation of thoracic and lumbar vertebral failure loads with in situ vs. ex situ dual energy X-ray absorptiometry. J Biomech 34:579–587

34. Gluer CC, Blake G, Lu Y, Blunt BA, Jergas M, Genant HK (1995) Accurate assessment of precision errors: how to measure the reproducibility of bone densitometry techniques. Osteoporos Int 5:262–270

35. Carballido-Gamio J, Folkesson J, Karampinos DC, Baum T, Link TM, Majumdar S, Krug R (2011) Generation of an atlas of the proximal femur and its application to trabecular bone analysis. Magn Reson Med 66:1181–1191

36. Krug R, Burghardt AJ, Majumdar S, Link TM (2010) High-resolution imaging techniques for the assessment of osteoporosis. Radiol Clin N Am 48:601–621

37. Ito M, Ikeda K, Nishiguchi M, Shindo H, Uetani M, Hosoi T, Orimo H (2005) Multi-detector row CT imaging of vertebral microstructure for evaluation of fracture risk. J Bone Miner Res 20:1828–1836

38. Chevalier Y, Quek E, Borah B, Gross G, Stewart J, Lang T, Zysset P (2010) Biomechanical effects of teriparatide in women with osteoporosis treated previously with alendronate and risedronate: results from quantitative computed tomography-based finite element analysis of the vertebral body. Bone 46:41–48

39. Graeff C, Chevalier Y, Charlebois M, Varga P, Pahr D, Nickelsen TN, Morlock MM, Gluer CC, Zysset PK (2009) Improvements in vertebral body strength under teriparatide treatment assessed in vivo by finite element analysis: results from the EUROFORS study. J Bone Miner Res 24:1672–1680

40. Keaveny TM, Donley DW, Hoffmann PF, Mitlak BH, Glass EV, San Martin JA (2007) Effects of teriparatide and alendronate on vertebral strength as assessed by finite element modeling of QCT scans in women with osteoporosis. J Bone Miner Res 22:149–157

41. Issever AS, Link TM, Kentenich M, Rogalla P, Burghardt AJ, Kazakia GJ, Majumdar S, Diederichs G (2010) Assessment of trabecular bone structure using MDCT: comparison of 64- and

320-slice CT using HR-pQCT as the reference standard. Eur Radiol 20:458–468

42. Augat P, Schorlemmer S (2006) The role of cortical bone and its microstructure in bone strength. Age Ageing 35:27–31

43. Noshchenko A, Plaseied A, Patel VV, Burger E, Baldini T, Yun L (2013) Correlation of vertebral strength topography with 3-dimensional computed tomographic structure. Spine (Phila Pa 1976) 38:339–349

44. Silva AC, Lawder HJ, Hara A, Kujak J, Pavlicek W (2010) Innovations in CT dose reduction strategy: application of the adaptive statistical iterative reconstruction algorithm. AJR Am J Roentgenol 194:191–199

45. Mulder L, van Rietbergen B, Noordhoek NJ, Ito K (2012) Determination of vertebral and femoral trabecular morphology and stiffness using a flat-panel C-arm-based CT approach. Bone 50:200–208

46. Bauer JS, Link TM, Burghardt A, Henning TD, Mueller D, Majumdar S, Prevrhal S (2007) Analysis of trabecular bone structure with multidetector spiral computed tomography in a simulated soft-tissue environment. Calcif Tissue Int 80:366–373

47. Lochmuller EM, Krefting N, Burklein D, Eckstein F (2001) Effect of fixation, soft-tissues, and scan projection on bone mineral measurements with dual energy X-ray absorptiometry (DXA). Calcif Tissue Int 68:140–145